Title

DNA origami patterning of synthetic T cell receptors reveals spatial control of the sensitivity and kinetics of signal activation

Authors

Dong, Rui
Aksel, Tural
Chan, Waipan
et al.

Publication Date

2021

DOI

10.1101/2021.03.12.434905

DNA origami patterning of synthetic T cell receptors reveals spatial control of the sensitivity and kinetics of signal activation

Rui Dong[a], Tural Aksel[a], Waipan Chan[b], Ronald N. Germain[b], Ronald D. Vale[a,c,1], and Shawn M. Douglas[a,1]

[a]Department of Cellular and Molecular Pharmacology, University of California, San Francisco, CA 94143; [b]Lymphocyte Biology Section, Laboratory of Immune System Biology, National Institute of Allergy and Infectious Diseases, NIH, Bethesda, MD 20892; and [c]HHMI, University of California, San Francisco, CA 94143

Edited by K. Christopher Garcia, Stanford University, Stanford, CA, and approved August 19, 2021 (received for review May 20, 2021)

Receptor clustering plays a key role in triggering cellular activation, but the relationship between the spatial configuration of clusters and the elicitation of downstream intracellular signals remains poorly understood. We developed a DNA-origami–based system that is easily adaptable to other cellular systems and enables rich interrogation of responses to a variety of spatially defined inputs. Using a chimeric antigen receptor (CAR) T cell model system with relevance to cancer therapy, we studied signaling dynamics at single-cell resolution. We found that the spatial arrangement of receptors determines the ligand density threshold for triggering and encodes the temporal kinetics of signaling activities. We also showed that signaling sensitivity of a small cluster of high-affinity ligands is enhanced when surrounded by nonstimulating low-affinity ligands. Our results suggest that cells measure spatial arrangements of ligands, translate that information into distinct signaling dynamics, and provide insights into engineering immunotherapies.

DNA origami | T cell signaling | chimeric antigen receptor T cell | immunotherapy | MAP kinase signaling

Cell-surface receptors transduce extracellular signals into intracellular responses. Higher-order assemblies of signaling molecules provide important mechanisms for regulating threshold responses, amplifying signals, and suppressing noise in signal transduction (1). The T cell receptor (TCR) is a well-studied example of high-order assembly. Upon receptor interaction with a peptide–major histocompatibility complex molecule (pMHC) ligand of sufficient strength, the immunoreceptor tyrosine activation motifs (ITAMs) in the TCRζ and associated CD3 chains undergo phosphorylation and recruit various signaling components into supramolecular microclusters of 30 to 300 nm in diameter (2, 3). Though sparsely distributed monomeric ligands were reported to be able to activate T cells (4–6), microclusters constitute important venues for signaling, as they facilitate the initiation and propagation of intracellular signals by increasing the local concentration of stimulatory enzymes and excluding the signaling inhibitory molecules (7–9).

While mounting evidence has established clustering as an important mechanism for regulating TCR signaling, limited information is available about the nanoscale structure of TCR microclusters. Understanding how spatial arrangement of pMHC-TCR interactions within clusters affects the signaling outcome has been particularly elusive. We aim to address these problems, for they provide insights about how cells convert extracellular stimuli into distinct cellular responses. Previous studies have manipulated the spatial arrangement of ligands via soluble cross-linker (10, 11), nanolithography (12–15), or two-dimensional protein array (16). While these approaches have provided important insights into spatial requirements of receptor–ligand engagement, their methods remain costly and technically demanding. They also have significant limitations for manipulating receptor–ligand affinity while also controlling reactions at the single-molecule nanometer scale, capacities needed for more refined interrogation of how cells convert extracellular stimuli into distinct cellular responses.

To address these challenges, we sought to design a system to achieve nanoscale manipulation of ligand patterns using DNA origami, a method that relies on numerous short DNA "staple" strands to fold a multikilobase-long "scaffold" DNA into nanoscale structures of customizable shape (17). Staple strands may also serve as handles for attaching diverse molecular components to enable novel types of biological experiments. We and others have used DNA origami to stimulate cells via patterned display of antibody fragments, peptides, or native ligands (18). However, relying on protein-based ligands introduces additional technical challenges, including incomplete functionalization and fine-tuning the strength and conformational preference of receptor–ligand interactions (18). Previously, we developed a synthetic T cell signaling system in which we replaced extracellular pMHC-TCR interaction with DNA hybridization (9), paving the way to develop a synthetic signaling system compatible with DNA origami structure. In this study, we combined these approaches, converting receptor–ligand interactions into DNA hybridization, which is highly tunable with DNA origami methods.

Here, we describe our results using a DNA origami signaling system compatible with live T cell imaging to investigate how specified nanometer arrangements of ligands affect MAP kinase

Significance

It has been proposed that the spatial arrangement of ligands plays a key role in regulating downstream intracellular signals. Because of methodological limitations in precise ligand patterning, however, the relationship between spatial configuration of clusters and signaling dynamics remains poorly understood. By developing a DNA-based molecular "pegboard" for ligand patterning, we demonstrated that the nanometer arrangement of ligands plays significant roles in modulating signal transduction in T cells. Ligand clustering not only affects the triggering sensitivity but also determines the temporal dynamics of the intracellular signaling response. Our approach is highly translatable for studying various signaling pathways, and our results provide insights into biomolecular engineering for therapeutic uses.

Author contributions: R.D., R.D.V., and S.M.D. designed research; R.D. and T.A. performed research; R.D., T.A., W.C., R.N.G., and S.M.D. contributed new reagents/analytic tools; R.D., R.D.V., and S.M.D. analyzed data; and R.D., R.D.V., and S.M.D. wrote the paper.

The authors declare no competing interest.

This article is a PNAS Direct Submission.

[1]To whom correspondence may be addressed. Email: valer@hhmi.org or shawn.douglas@gmail.com.

This article contains supporting information online at https://www.pnas.org/lookup/suppl/doi:10.1073/pnas.2109057118/-/DCSupplemental.

Published September 29, 2021.

(MAPK) signaling dynamics. For this purpose, we chose an engineered receptor system (chimeric antigen receptor, or CAR) that replaced the usual αβ-TCR of the T cell with an intracellular domain derived from CD86 and the ζ-chain ITAMs to simulate the clinically important CAR-T cell systems used increasingly in cancer immunotherapy. Using this model, we found that the number and spacing of ligands within each microcluster modifies the triggering threshold and the time course of the MAPK signaling response. Specifically, ligand spacing affects the initiation time of the MAPK response, and the ligand cluster size determines the duration of the MAPK signal. These findings have important implications for both the downstream effects of MAPK signaling on gene expression and also on the reported role of activated MAPK in feedback regulation of TCR ligand discrimination (19, 20). Low-affinity ligands, though nonstimulatory on their own, also can enhance the sensitivity of MAPK signaling when placed adjacent to stimulatory high-affinity ligands. Our results demonstrate the versatility of DNA origami in dissecting the mechanisms of transmembrane signaling and reveal the role of nanoscale ligand organization in modulating the T cell signaling response.

Results

Design and Characterization of DNA Origami "Pegboard" for Ligand Presentation. Previously, we developed a synthetic T cell signaling system in which extracellular DNA hybridization acts as the receptor–ligand interaction to trigger T cell signaling (9). In this system, the native TCR was replaced by a DNA-based chimeric antigen receptor (DNA-CARζ) that contains an intracellular CD3-ζ chain, a transmembrane domain from CD86, and an extracellular SNAP tag protein that covalently reacts with a benzylguanine–labeled single-stranded DNA (ssDNA, "receptor strand"). DNA hybridization between receptor ssDNA with the complementary ligand ssDNA attached on the planar lipid bilayer triggers the phosphorylation of the ITAM domains of the CD3-ζ and thus downstream T cell signaling.

To develop a DNA origami structure that can successfully control T cell ligand patterning, we designed a nanoscale pegboard that employs the ssDNA ligands as "pegs" and the DNA-CARζ as the cell-surface receptor (Fig. 1*A*). The DNA origami pegboard is a square plate with dimensions of 60 × 60 nm with a height of 6 nm (Fig. 1*B*). The structure has a two-layer design based on a honeycomb-lattice architecture (21), which offers higher rigidity than a single-layer design. The pegboard has 72 "peg" DNA sticky ends facing the top side of the plate, which can each be extended with additional nucleotides to incorporate the ligand DNA of custom length and sequence (*SI Appendix*, Fig. S1*C*). The 72 peg staples are arranged in a 6 × 12 array with rows and columns spaced at 7-nm or 3.5-nm intervals (Fig. 1*B*), respectively, which enables interligand spacing from up to 38.5 nm to 3.5 nm. We also added 12 biotin staple DNAs at the bottom side of the pegboard for attachment to streptavidin-coated surfaces and ATTO647N fluorophores at the four corners of the DNA pegboard for visualization (Fig. 1*B* and *SI Appendix*, Fig. S1 *A* and *B*). Total internal reflection fluorescence (TIRF) microscopy revealed that individual DNA origami particles also displayed relatively uniform patterns with respect to size (diffraction-limited) and intensity, suggesting a uniform structure with little aggregation (Fig. 1 *E* and *H* and *SI Appendix*, Fig. S2*B*; variations were mainly attributable to fluorescence blinking). Photobleaching revealed four step-wise decreases in fluorescence intensity, in which four consecutive bleaching events were identified (Fig. 1*C*), consistent with the four-dye design. The DNA origami structure appeared to be properly folded when analyzed by agarose gel (*SI Appendix*, Fig. S2*D*) and negative stain transmission electron microscopy (TEM) (Fig. 1*D* and *SI Appendix*, Fig. S2*E*) and had no obvious defects, deformation, or aggregation.

We then examined whether the ssDNA ligand strands on the origami are capable of binding ssDNA receptor strands. DNA pegboards carrying the ligand strands recruited the receptor strands (*SI Appendix*, Fig. S2 *A* and *B*). The amount of receptor strands recruited was linearly proportional to the number of ligands per DNA origami as intended (*SI Appendix*, Fig. S2*C*).

Triggering T Cell Signaling Using DNA Origami Nanostructures. Next, we examined whether the receptor DNAs on the T cell surface respond to DNA origami–carried ligands (Fig. 1*E*). We used a 16-nucleotide DNA as the ligand strand that generates a high-affinity interaction (predicted off-rate > 7 h). This high-affinity interaction was selected to simulate the binding of an avid antibody-combining domain to its molecular target, as occurs in CAR T Cell immunotherapy (22). We immobilized the DNA pegboards on a glass surface via biotin–streptavidin–biotin interactions and loaded Jurkat cells expressing DNA-CARζ-GFP to visualize receptor clustering (Fig. 1*A*). The predicted DNA origami ligand–receptor dimension between cell surface and glass surface is estimated at ∼26.7 nm [3.2 nm for SNAP tag (23), ∼5.4 nm for 16-mer hybridized receptor–ligand DNA (9), 6 nm for the thickness of the DNA pegboard, 5 nm for streptavidin (24), and 7.1 nm for biotin-BSA (25)]. The DNA pegboards recruited DNA-CARζ-GFP into submicron clusters (Fig. 1*E*). The amount of DNA-CARζ-GFP recruited per DNA origami particle was proportional to the number of ligands per DNA pegboard (Fig. 1*F*). Together, these results suggest that DNA origami can fine-tune the number of engaged ligand–receptor pairs on the T cell surface.

We then examined whether the DNA pegboard could transmit intracellular signals. TCR-pMHC interaction leads to the TCR phosphorylation, which triggers the recruitment of ZAP70, a cytosolic kinase that phosphorylates downstream targets. We tested our concept using 72-ligand DNA pegboard, which holds maximal capacity for receptor binding and thus optimizes the signal-to-noise ratio for ZAP70-mScarlet recruitment. We observed a robust recruitment of ZAP70-mScarlet to DNA-CARζ-GFP microclusters engaged by DNA origami particles (Fig. 1 *H*–*J*). Interestingly, ZAP70 exhibits a robust initial recruitment over the first 2 min, with recruitment then decreasing to 25% to 50% of the peak intensity over the next ∼3 min (*SI Appendix*, Fig. S3*A* and Movie S1). The decline is unlikely due to photobleaching or special properties of mScarlet, because when we compared ZAP70-GFP and DNA-CARζ-GFP, ZAP70-GFP exhibited similar behavior, whereas DNA-CARζ-GFP showed no decline in fluorescence over this time period (*SI Appendix*, Fig. S3*B* and Movie S2) but is consistent with several reports of TCR-induced SHP-1 phosphatase recruitment and dephosphorylation of several substrates in the engaged TCR complex (19, 26, 27). DNA pegboards carrying as few as nine ligand DNA strands also demonstrated clear recruitment of ZAP70 (*SI Appendix*, Fig. S4*B*). However, due to the background fluorescence of cytosolic ZAP70 (either mScarlet or GFP fusion), we could not consistently and reliably identify ZAP70 microclusters triggered by DNA pegboards carrying six or fewer ligand DNA strands.

TCR triggering by pMHC induces the nucleation and retrograde flow of the actin network, which carries TCR microclusters to the cell center (28). To examine whether ligated DNA pegboards become coupled to the actin retrograde flow as described for the native TCR, we attached DNA origami structures onto a planar supported lipid bilayer containing biotinylated lipids rather than fixing them onto glass (*SI Appendix*, Fig. S4*A*). Time-lapse images revealed that these mobile DNA origami pegboards, in complex with the DNA-CARζ microclusters, moved centripetally toward the cell center, forming the "bull's eye" structure typical of an immunological synapse (*SI Appendix*, Fig. S4*C* and Movie S3). In summary, these results indicate that DNA pegboards are capable of triggering proximal intracellular signaling typical of the TCR.

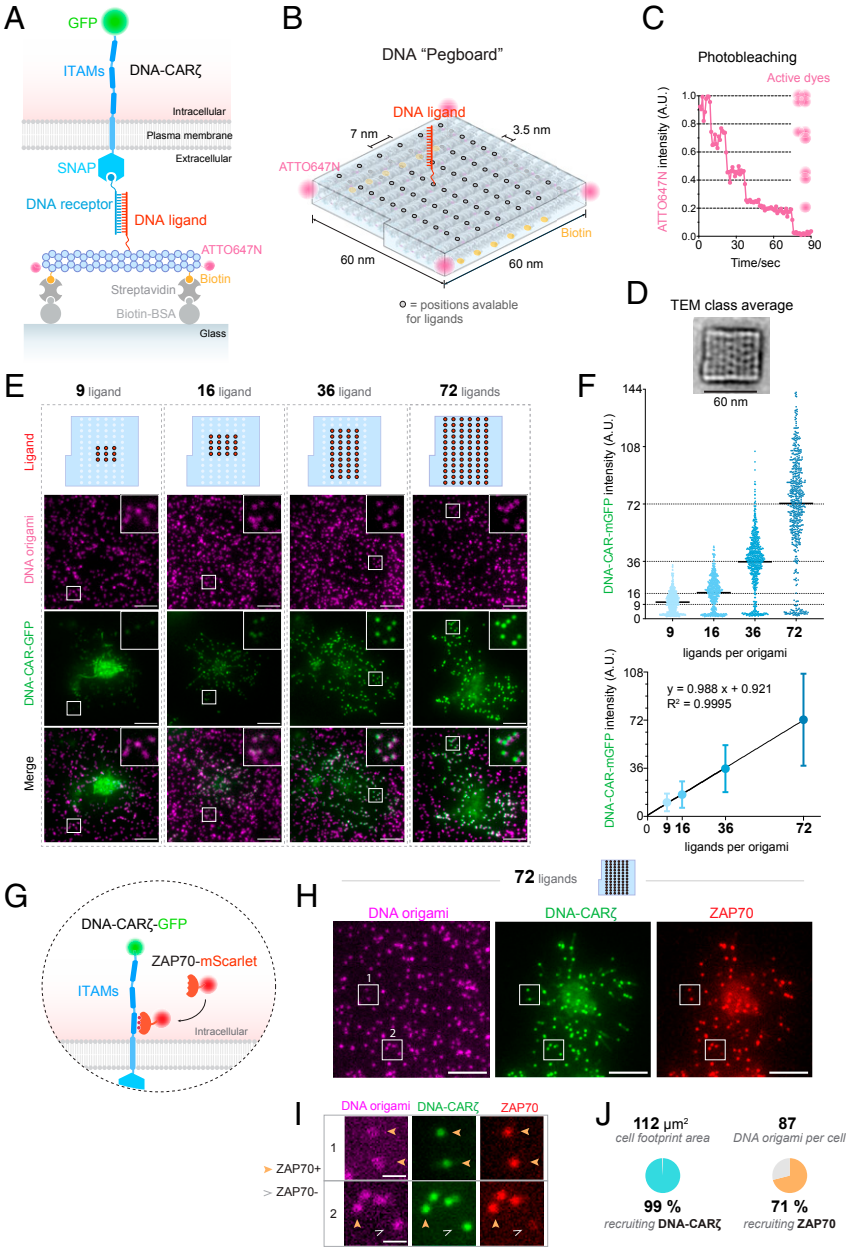

Fig. 1. Design of the DNA origami pegboard for patterned display of ligands capable of triggering T cell signaling. (*A*) Schematic of our DNA origami–based T cell activation system. The native TCR is replaced by a DNA-CARζ composed of an intracellular CD3-ζ chain fused with GFP, a transmembrane domain from CD86, and an extracellular SNAP tag protein covalently reacting with a benzyl-guanine–labeled ssDNA ("DNA receptor"). ssDNAs complementary to the receptor strands ("DNA ligands") are displayed with a customizable pattern on a pegboard-shaped DNA origami, which is immobilized on a glass coverslip via biotin–streptavidin–biotin–BSA interactions and labeled with ATTO647N for fluorescence microscopy. (*B*) Designing details of the DNA pegboard. The DNA origami pegboard is roughly a square shape of 60 × 60 nm^2. The 72 staple DNAs of customizable length and sequence on the top of the DNA pegboard present maximum 72 DNA ligands in a 6 × 12 array at 7-nm or 3.5-nm intervals, respectively. Four ATTO647N dyes label the corners for fluorescence microscopy, and two rows of six biotin moieties label the bottom for mounting on a glass coverslip via biotin–streptavidin interactions. (*C*) Fluorescence photobleaching curve for one DNA origami particle. Note the five decreasing steps, which signify the bleaching events of the four ATTO647N fluorophores in succession. A.U., artificial unit. (*D*) Class averaging of the TEM image of the DNA origami. (Scale bar: 60 nm.) (*E*) TIRFM images of ATTO647N-labeled DNA origami and DNA-CARζ-GFP clusters in Jurkat T cells. DNA-CARζ-GFP fluorescence intensity per DNA origami particle decreases as the number of ligands per DNA origami reduces. Insets show colocalization of DNA-CARζ-GFP microclusters with DNA origami particles. (Scale bar: 5 μm.) (*F*) DNA-CARζ-GFP fluorescence intensity per DNA origami particle was quantified and plotted as scattered dots (*Top*, solid bars indicate the mean). Fitting with a linear regression model suggests that the mean DNA-CARζ-GFP fluorescence intensity is linearly proportional to the number of ligands per DNA origami (*Bottom*, data were presented as mean ± SD). (*G–J*) ZAP70 is recruited to a subset of DNA pegboard–induced receptor microclusters. (*G*) Schematic of the cell line used in *H–J*. Jurkat cells coexpress DNA-CARζ-GFP and ZAP70-mScarlet. Ligand–receptor interaction triggers tyrosine phosphorylation of the ITAM domains of the DNA-CARζ-GFP, which recruits ZAP70-mScarlet. (*H* and *I*) TIRF microscopy images of a Jurkat cell stimulated by 72-ligand DNA origami particles showing ZAP70-mScarlet recruitment to a subset of DNA-CARζ-GFP microclusters. (Scale bar: 5 μm.) Boxed regions in *H* were magnified in *I*, showing that some DNA origami particles recruit DNA-CARζ and ZAP70 (solid yellow arrowheads), while some other DNA origami particles recruit DNA-CARζ but lack ZAP70 (hollow gray arrowheads). (*J*) A total of 1,046 72-ligand DNA origami particles covered by 12 cells were examined for the percentage of recruiting DNA-CARζ and ZAP70 clustering. While the great majority (99.22 ± 1.21%) of all DNA origami particles trigger DNA-CARζ clustering, only a subset (71.04 ± 17.14%) of them recruit ZAP70.

DNA Origami Pegboard Revealed ERK Triggering Depends on Ligand Density. ZAP70 activation induces the recruitment of a supramolecular signalosome consisting of various signaling molecules, including LAT, Grb2, and SOS, which activates the Ras-Raf-Mek-ERK (MAPK) pathway that activates gene expression and also has been reported to act in a positive-feedback manner to support effective TCR signaling (19, 20). To measure ERK activation by DNA pegboards, we engineered a version of Jurkat T cells expressing both the DNA-CARζ and a kinase translocation reporter (KTR) that enables monitoring of ERK activities with high sensitivity in single living cells (29). Upon phosphorylation, this reporter is exported from the nucleus to the cytosol and returns to the nucleus upon dephosphorylation (Fig. 2*A*). We observed ERK-KTR translocation in 33% cells stimulated with 72-ligand DNA pegboards after 12 min, in contrast to a background of 6% cells resting on a surface with zero-ligand DNA pegboards (Fig. 2*B*).

Next, we sought to understand the impact of nanoscale organization of ligands on the probability of triggering ERK signaling. Specifically, we asked how many ligands per cluster were minimally required to achieve signaling competence and whether the spatial patterning of these ligands made a difference.

To address ligand number, we designed DNA pegboards that carried various numbers of strands (Fig. 2 *C*, *Top*) and compared their probabilities of triggering the ERK response within 12 min over a range of origami densities (Fig. 2 *C*, *Bottom Left*). One- and two-ligand DNA pegboards were not capable of triggering an ERK response that was significantly greater than the zero-ligand DNA pegboard control at the densities up to two origami per square micrometer, which is about 200 origami per cell. At the same DNA pegboard density (two four-ligand DNA origami per square micrometer), the four-ligand DNA pegboard significantly increased the probability of ERK activation (30% of cells). Similar probability of ERK activation was achieved by DNA pegboards that had higher ligand occupancy when presented at lower density (one 16- and 72-ligand DNA origami per square micrometer). In short, increased ligand occupancy per DNA pegboard increases ERK triggering sensitivity.

Next, we asked whether cells control their activation by measuring the overall number of ligands or the spatial pattern (number of clusters and/or ligands occupancy per cluster). We explored this question by replotting the dose–response curves by various DNA pegboards in terms of the overall number of ligands presented across cell contact area (Fig. 2 *C*, *Bottom Right*). At the same DNA ligand density (2∼8 DNA ligands per square micrometer), the four-ligand DNA pegboard increased the probability of ERK activation compared to the two- or one-ligand DNA pegboards, suggesting that the ligand clustering improves ERK signaling sensitivity. As ligand occupancy per cluster further increased, they became less efficient in triggering ERK response. When the overall ligand density remained constant (∼10 ligands per square micrometer), the 72-ligand DNA pegboards triggered 10% of cells, while the 16- or 4-ligand DNA pegboards triggered 20% and 30%, respectively. Overall, these results suggest that the spatial arrangement of ligands alters the threshold for T cell activation. In concert with the preceding data on the effect of ligand number, these findings indicate that there is a narrow window of local ligand density that is optimal for receptor signaling. Increased overall T cell response thus seems to involve summing suprathreshold events among receptors engaging distinct small ligand clusters.

Ligand Clustering Encodes the Time Course for the ERK Response. The single-cell KTR reporter assay reveals information about the timing, amplitude, and cell-to-cell variation of ERK signaling (Fig. 3*A*). Inspired by a growing body of evidence showing that the ERK pathway generates time-varying signals in response to different input stimuli in nonhematopoietic cells (30–33), we examined the time courses of ERK signals in T cells stimulated by a variety of ligand patterns.

Keeping the overall number of ligands presented across cell contact area the same, we varied the ligand density per origami and examined the impact of cluster size on ERK signaling (Fig. 3*B*). Under the conditions of ∼34 to 42 ligands per square micrometer, a similar fraction (∼42%) of cells were activated by 4-, 16-, or 72-ligand DNA pegboards at varied densities over 96-min duration (Fig. 3*C*). ERK signals in active cells were triggered within a similar period of time and reached a similar ERK signal magnitude (Fig. 3*D*). However, remarkably, the ERK signal stimulated by the 72-ligand DNA pegboards terminated significantly earlier than the 4- and 16-ligand DNA pegboards. For example, only 10% of ERK-active cells (4% of all cells) exposed to 72-ligand origami still maintained an ERK signal at 36 min, compared to 77% of ERK-active cells (35% of all cells) exposed to the 4-ligand origami (Fig. 3 *C* and *D*). In summary, our experiments reveal that ligand patterning affects the duration of the ERK response.

Ligand Spacing Affects ERK Signaling. We next sought to define the impact of ligand spacing on the probability of activating ERK. With a four-ligand unit, we separated the ligands by 10 nm ("tight") or 40 nm apart ("sparse"). We also compared these two four-ligand origami platforms to single-ligand origamis at the same overall ligand density (Fig. 4 *A*, *Top*). In an experiment in which the origami density varied, the tight four-ligand origami was more potent than the sparse four-ligand origami (Fig. 4 *A*, *Bottom*). The sparse four-ligand origami was only minimally more potent than the single-ligand origami when compared at a similar overall ligand density. When we examined the kinetics of ERK signaling at an equal overall ligand density (Fig. 4*B*), we found that the tight four-ligand origami has a faster ERK response time than the sparser origamis (Fig. 4*C*), although the duration and the magnitude of the ERK signal were similar (Fig. 4*D*). These results reveal that a denser packing of ligands leads to a faster and more efficacious ERK response.

Closely Adjacent Weak Ligands Synergize with Strong Ligands to Produce ERK Responses. When a T cell scans the surface of an antigen-presenting cell using its physiologic αβ-TCR, it encounters a small number of high-affinity antigenic peptide-MHCs amid a large number of endogenous peptide-MHCs with low affinity (34). This situation is typical for the recognition of tumor-associated antigens, which are usually expressed in extremely low levels (due to defects in their antigen processing and presentation machinery) among the vast pool of low-affinity self-peptides on the tumor cell surface (35). Some studies have reported that low-affinity pMHC ligands promote signaling by agonist pMHC (11, 20, 36), whereas experiments conducted under other experimental conditions observed no substantial effect of such low affinity ligands in T cell activation (20, 37).

Because most engineered CAR-T cells retain expression of an αβ-TCR in addition to the antibody-based CAR, we utilized our model system to explore if weak self-ligand interactions that might occur when such CAR-T cells encounter a tumor could facilitate signaling. We reinvestigated this question by leveraging the modularity of the DNA origami pegboard design, which allows for ligands of different affinities to be patterned in an addressable fashion. To model low affinity TCR binding, we decreased the number of hybridizing nucleotides on the ligand strand from 16 to 11 while maintaining the overall length with additional unhybridized thymine nucleotides (Fig. 5 *A*, *Top*). While the half-life for dissociation of 16-mer DNA duplex is >7 h, the 11-mer duplex dissociates with a much faster half-life of ∼2 s for the 11-mer (9), similar to pMHC binding to some TCRs (38).

To test the effect of additional low-affinity ligands in the presence of strong agonist ligands, we created a DNA pegboard

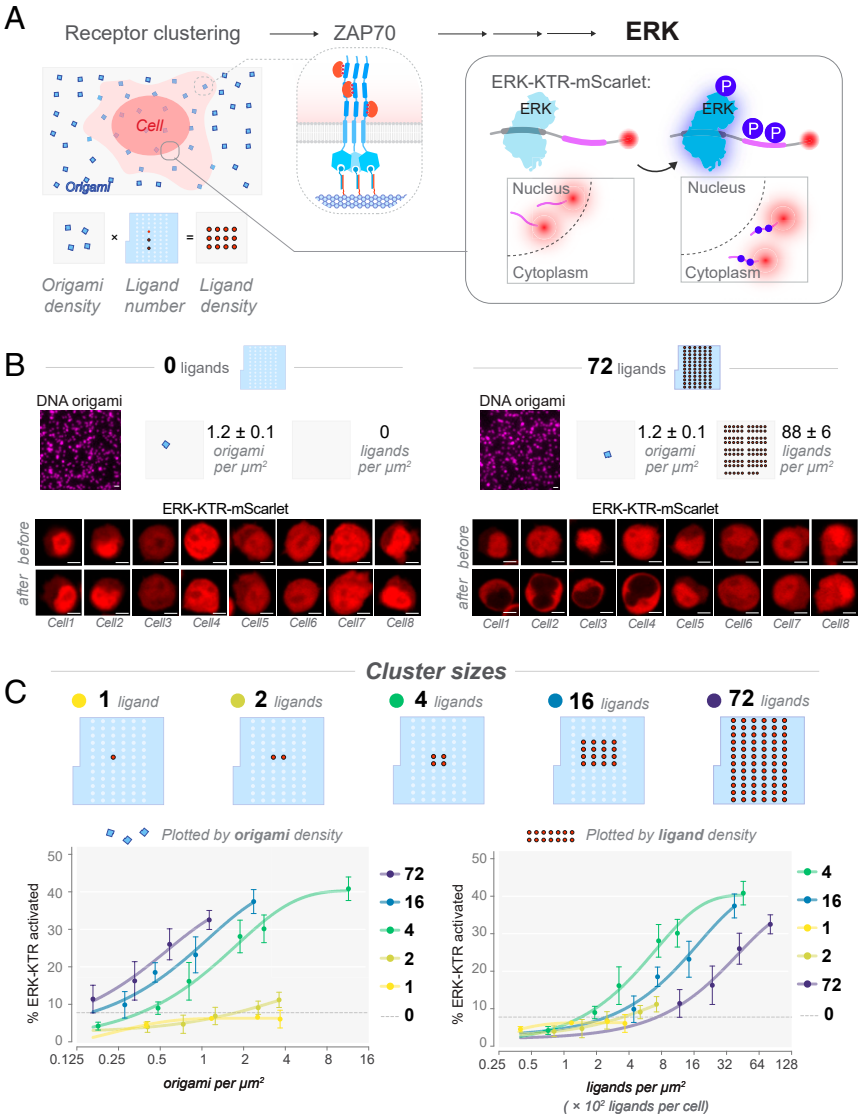

Fig. 2. Display patterns modify the threshold ligand density to trigger ERK signaling. (*A*) Schematic workflow for the inspection of ERK signaling in response to DNA origami ligands displayed at a prescribed pattern. DNA origami particles were immobilized on the glass bottom of multiwell plates. DNA origami density was determined by TIRF microscopy, based on which the overall density of the ssDNA ligands was inferred (*Left*). ERK signaling activities in cells stimulated by DNA origami ligands were monitored with the ERK-KTR-mScarlet reporter, which converts phosphorylation into a nucleus-to-cytoplasm translocation event (*Right*). (*B*) Representative results from the workflow in *A*. DNA origami pegboards that carry either 0 or 72 DNA ligands were plated at equal density as measured by TIRF (*Top*). (Scale bar: 1 μm.) Jurkat cells coexpressing DNA-CARζ-GFP and ERK-KTR-mScarlet were introduced onto the DNA origami–coated glass-bottom imaging plate, and the ERK-KTR-mScarlet translocation was monitored with confocal microscopy (*Bottom*). (Scale bar: 5 μm.) Eight representative cells stimulated by either 0- or 72-ligand DNA origami were shown ("before": cell landing; "after": 18 min after cell landing). Note that 72-ligand DNA origami pegboards induced ERK-KTR translocation in a fraction of cells, whereas the 0-ligand DNA origami control did not produce such activities. (*C*) Impact of number of ligands per cluster on the probability of triggering ERK. DNA pegboards carrying varying ligand layouts (*Top*) were used to stimulated Jurkat cells coexpressing DNA-CARζ and ERK-KTR. The ERK-KTR activation was monitored every 12 min over 96 min. A C:N ratio of 2.5 was set as the threshold of ERK-KTR activation. Percentages of ERK-KTR activation were calculated at 12 min after cell landing and plotted in terms of the DNA origami density (*Bottom Left*) or of the overall ligand density (*Bottom Right*). The estimated numbers of ligands per cell are calculated by multiplying the overall ligand density by the averaged cell footprint area (100 μm^2). Each data point represents the mean ± SD of three independent replicates (>100 cells scored per replicate). Data were pooled from two sets of experiments: one includes the one-, two-, and four-ligand DNA origami, and the other includes the 4-, 16- and 72-ligand DNA origami. Data for four-ligand DNA origami from both experiments were shown, for which the results at the same DNA origami density match between two experiments and are shown as average.

on which 4 high-affinity ligand strands (16-mer) were placed in the center, surrounded by 68 low-affinity ligand strands (11-mer) (Fig. 5*A*, blue box). To directly test the adjacency effect and rule out the possibility that additional low-affinity ligands may collectively increase the signaling by adhesion or other means, we included a condition in which the high-affinity ligands were spatially distant from the low-affinity ligands on separate DNA pegboards (Fig. 5*A*, orange box). We examined the probability of activating ERK with these ligand arrangements at extremely low ligand density, when neither the four-ligand high-affinity DNA pegboard nor the 72-ligand low-affinity DNA pegboard triggers ERK (Fig. 2*C*). The results reveal that the presence of 68 low-affinity ligands that surround the 4 high-affinity ligands heightened the probability of ERK activation (Fig. 5*B*). An elevated ERK response was not observed when high- and low-affinity ligands were placed on separate DNA pegboards, suggesting that the synergistic effect requires proximity on a nanometer scale. We also compared the kinetics of ERK signaling in cells

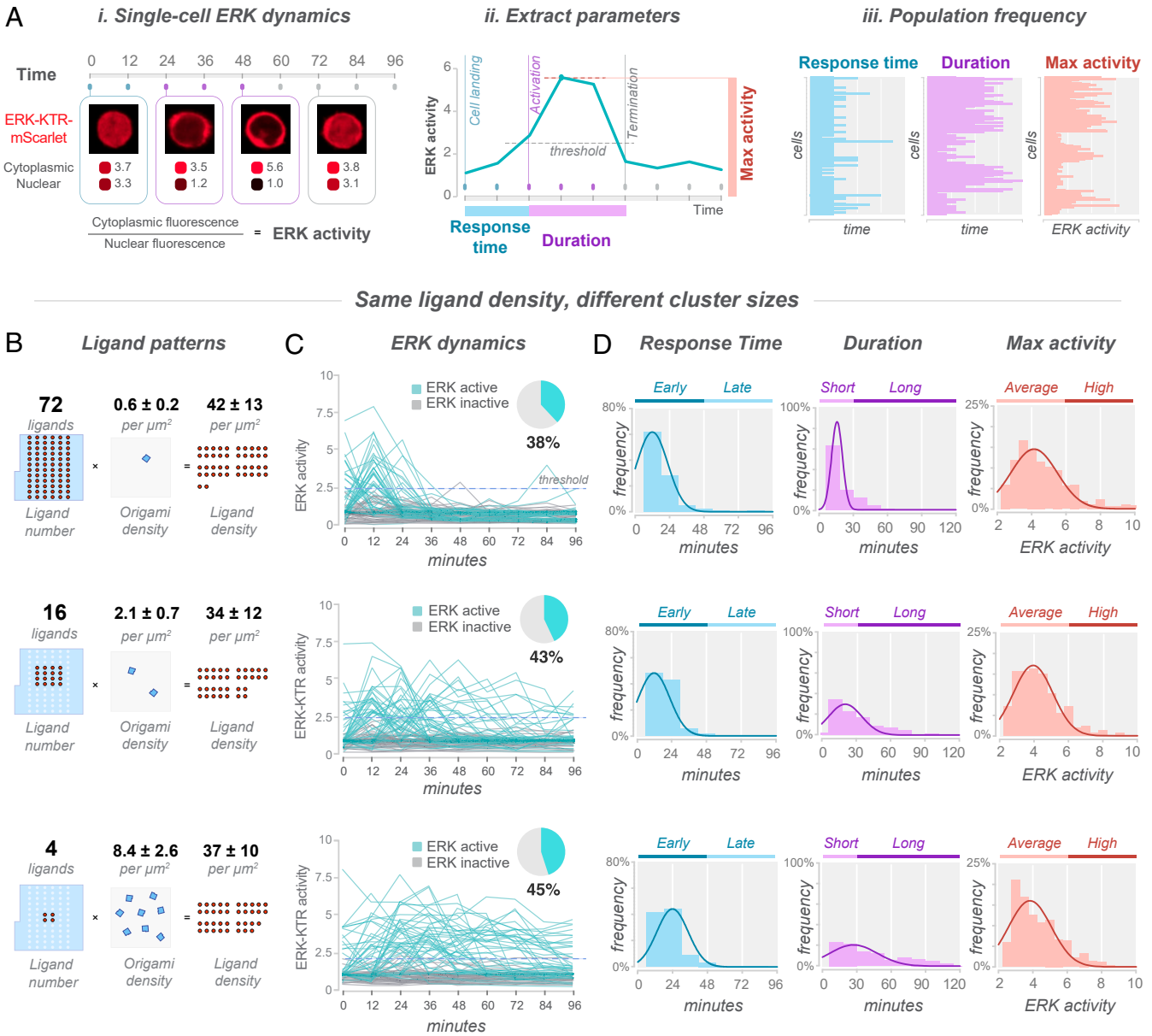

Fig. 3. Ligand cluster size encodes the temporal course of ERK response. (*A*) Schematic showing the approaches of monitoring single-cell ERK activity dynamics and extracting key parameters for population-wise analysis. ERK activity was monitored at 12-min intervals for 96 min (see *SI Appendix*, Fig. S5 for additional notes) and calculated by the cytoplasmic-to-nuclear ratio of the ERK-KTR-mScarlet fluorescence intensity. A C:N ratio of 2.5 was set as the threshold for ERK activation. Response time is defined as the time spent from cell landing to ERK-KTR activation. Duration of activation is defined as the length of time of ERK-KTR being positive. Maximal ERK activity was scored as the maximal C:N ratio of ERK-KTR fluorescence intensity. (*B–D*) The number of ligands per cluster governs the duration of ERK activation. (*B*) Diagrams of the DNA origamis used in *C* and *D*. DNA origamis with varying numbers of ligands were immobilized on glass at respective densities so that they reached similar overall ligand densities. (*C*) Single-cell ERK dynamics stimulated with the DNA origami as indicated in *B*. ERK-KTR activity traces of 100 cells were shown for each dataset, with the ERK-active cells highlighted in cyan and ERK-inactive cells in gray. Note the sustained ERK-KTR activities in cells stimulated by the 16- or 4-ligand DNA origami, in contrast to the rapid termination of ERK-KTR activity in cells stimulated by the 72-ligand DNA origami. The pie charts indicate the percentages of ERK-active cells, which were calculated over the 96-min duration of $n >$ 600 cells pooled from three independent experiments. (*D*) Duration of activation, response time, and maximal activity scored as illustrated in *A*. For each dataset, $n = 250$ ERK-activated cells pooled from three independent experiments. Mean ± SD: (i) response time: "72-ligand", 18.75 ± 11.49 min; "16-ligand", 20.01 ± 10.63 min; "4-ligand", 23.28 ± 13.82 min. (ii) Duration: "72-ligand", 19.42 ± 11.32 min; "16-ligand", 30.79 ± 20.88 min; "4-ligand", 41.83 ± 27.88 min. (iii) max activity (C:N ratio): "72-ligand", 4.671 ± 1.634; "16-ligand", 4.313 ± 1.266; "4-ligand", 4.285 ± 1.312.

stimulated with four high-affinity ligand clusters with or without surrounding low-affinity ligands (Fig. 5*C*). We chose a higher ligand concentration at which the four high-affinity ligand clusters trigger on their own so that more data were collected for the active cells. We observed similar single-cell ERK dynamics with respect to the amplitude, duration, or response time of ERK response (Fig. 5*D*). These results suggest that proximal low-affinity ligands sensitize the cell to stimulation by high-affinity ligands but do not change timing or amplitude of the ERK response.

Discussion

In this study, we demonstrated that DNA origami is a powerful method for interrogating cell signaling. Compared to nanolithography

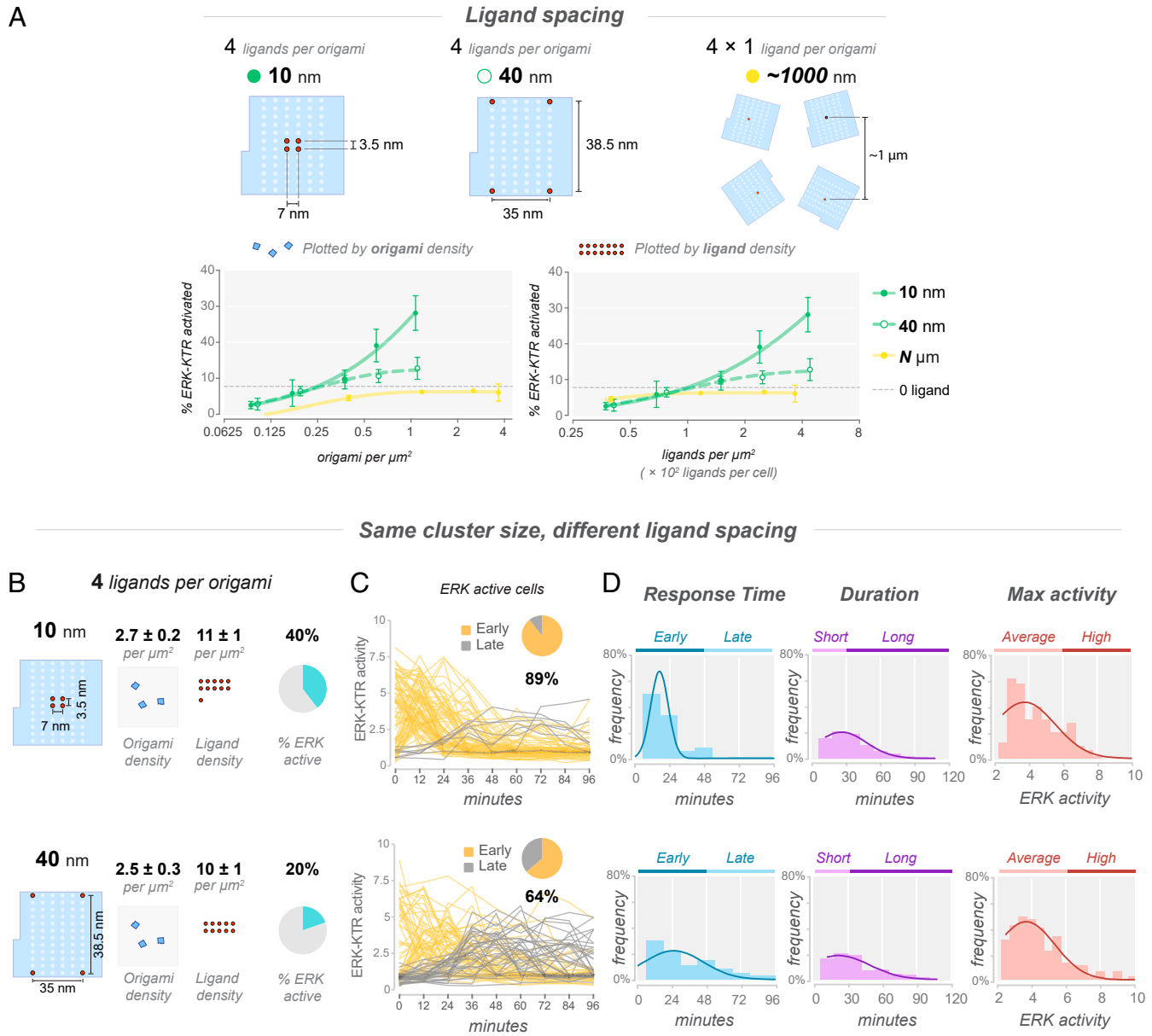

Fig. 4. Ligand spacing modifies ERK signaling threshold and timing. (*A*) Impact of ligand spacing on the probability of triggering ERK. DNA pegboards carrying varying ligand layouts (*Top*) were used to stimulated Jurkat cells coexpressing DNA-CARζ and ERK-KTR. The ERK-KTR activation was monitored every 12 min over 96 min. A C:N of 2.5 was set as the threshold of ERK-KTR activation. Percentages of ERK-KTR activation were calculated at 12 min after cell landing and plotted in terms of the DNA origami density (*Bottom Left*) or of the overall ligand density (*Bottom Right*). The estimated numbers of ligands per cell are calculated by multiplying the overall ligand density by the averaged cell footprint area (100 μm^2). Each data point represents the mean ± SD of three independent replicates (>100 cells scored per replicate). Data were pooled from two sets of experiments: one includes the four-ligand DNA origami with 10-nm or 40-nm spacing, and the other includes the four-ligand DNA origami with 10-nm spacing and one-ligand DNA origami with ~1-μm spacing. Data for four-ligand DNA origami from both experiments were shown, for which the results at the same DNA origami density match between two experiments and are shown as the average. (*B*) Diagram of the DNA origami particles used in *C* and *D*. Both DNA origamis carry four ligands but at different interligand spacing and were immobilized on glass at a similar density. (*C*) Single-cell ERK-KTR activities of 100 ERK-active cells were shown for each dataset. Traces of cells that initiate ERK activation within 48 min after cell landing were colored in yellow and those later than 48 min in gray. (*D*) Response time, duration of activation, and max activity of ERK-KTR activities in cells activated with the indicated DNA origami in *B*. Data were pooled from three independent experiments. n = 120 ERK-active cells out of 305 cells stimulated by the "10-nm" DNA origami and 120 ERK-active cells out of 571 cells by the "40-nm" DNA origami. Mean ± SD: i) response time: "10 nm," 24.06 ± 14.69 min; "40 nm," 40.31 ± 24.27 min; ii) duration: "10 nm," 35.40 ± 19.96 min; "40 nm," 37.42 ± 22.43 min; iii) max activity (C:N ratio): "dense," 4.468 ± 1.440; "sparse," 4.475 ± 1.536.

or protein two-dimensional (2D) arrays, our DNA origami–based approach offers the following advantages: 1) The DNA origami enables precise patterning over a few nanometers, within the size range of a native TCR-CD3 complex (~7.5 nm in diameter) (39). Conversely, the smallest nanolithography feature varies from 25 nm (15) to 40 nm (13). 2) The programmability and modularity of DNA structures enables simple control over multivalence, affinity, and spatial arrangement, which would otherwise involve complicated protein engineering via nanolithography or protein 2D arrays. Using DNA origami, we demonstrate how ligand spacing, number, and affinity affects the threshold and kinetics of the MAPK signaling response.

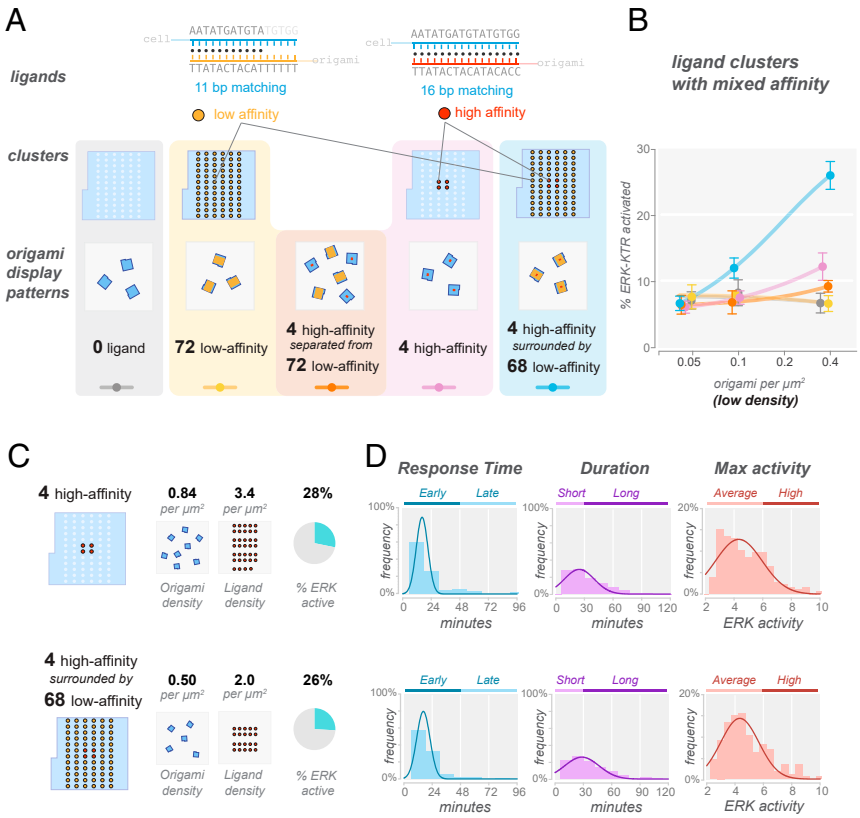

Fig. 5. Closely adjacent weak ligands enhance sensitivity of the strong ligands. (*A*) Schematic of the design and display patterns of DNA origami particles used in *B*. (*Top*) As a proxy for ligands with different affinity, the numbers of hybridizing nucleotides in the ligand strands varied from 11 bp to 16 bp. (*Middle*) Four types of DNA origamis were designed, with the 16-mer, 11-mer, or 0-mer ligand strands patterned as illustrated. (*Bottom*) DNA origamis were plated on glass with the five indicated arrangements. Note that the overall density of the 16-mer ligands was the same among "4 high-affinity separated from 72 low-affinity" (orange), "4 high-affinity" (pink), and "4 high-affinity surrounded by 68 low-affinity" (blue) groups. (*B*) Dose–response curves for the five types of DNA origami arrangements in *A*. Data were plotted by the overall DNA origami density, except for the "4 high-affinity separated from 72 low-affinity" dataset (orange), which was plotted by the density of four high-affinity ligand DNA origami only. Data are shown as mean ± SD of three independent replicates (>100 cells scored per replicate for each data point). (*C* and *D*) Additional low-affinity ligand at close adjacency to the high-affinity ligand does not modify the time course or the amplitude of ERK activities. (*C*) Schematics of the design and displaying density of the DNA origami particles used for *D*. The "4 high-affinity" or the "4 high-affinity surrounded by 68 low-affinity" DNA origami particles were plated at the specified density so that they reached a similar probability of ERK activation (data shown as mean ± SD of three independent replicates). (*D*) Frequency distribution of the duration, response time, and maximal activity of ERK stimulated by the DNA origami illustrated in *C*. $n > 170$ ERK-active cells out of >700 cells pooled from three independent experiments were included in the analyses. Mean ± SD: (i) response time: "4 high-affinity," 21.68 ± 18.12 min; "4 high-affinity surrounded by 68 low-affinity," 19.18 ± 11.02 min; (ii) duration: "4 high-affinity," 32.10 ± 19.30 min; "4 high-affinity surrounded by 68 low-affinity," 34.97 ± 20.47 min; (iii) max activity (C:N ratio): "4 high-affinity," 4.732 ± 1.564; "4 high-affinity surrounded by 68 low-affinity," 4.815 ± 1.548.

Ligand Nanoclustering Lowers the Threshold for Triggering ERK Signaling. Previous studies have shown that single ligand-bound DNA-CARζs without a DNA origami scaffold do not stably recruit ZAP70 and do not efficiently activate ERK (9). However, when ligated DNA-CARζs form small clusters, ZAP70 is recruited, which translates into a higher probability of ERK activation (9). It was speculated that the DNA-CARζ clusters more efficiently exclude the transmembrane CD45 phosphatase, leading to receptor phosphorylation by the Src family kinase LCK and ZAP70 recruitment. In these earlier experiments, clusters of DNA-CARζs formed naturally, and the distances between receptors could not be measured or controlled. In the present study, we could control ligand spacing. Our results are generally consistent with the idea that receptor clustering lowers the threshold for signaling. For example, we found that a tight cluster of four ligands (10-nm spacing) signals more efficiently than a sparser cluster size (40-nm spacing) (Fig. 4*A*). This result is generally consistent with previous experiments using nanolithographic structures by Cai et al. (13) showing that ligand clustering promotes signaling, although these structures could only probe ligand distancing down to 40 nm (13). A super-resolution microscopic study also reported that endogenous TCR clusters trigger signaling when interligand spacing decreases from 17 nm to 10 nm, although this study was correlative and did not manipulate spacing (40).

A recent study by Hellmeier et al. also examined the effect of ligand spacing on T cell signaling using DNA origami. In their study, they used either antibodies or pMHCs as ligands interacting with the native TCR instead of a CAR and measured calcium activation for their signaling response. They also used either one or two ligands on different-sized DNA origami platforms and, in the case of two ligands, varied the spacing between the ligands. Using antibodies as ligands, they reached similar conclusions to our study regarding sensitivity. Specifically, one-ligand platforms were inefficient, and for two-ligand origamis, decreasing the spacing between ligands from 48 nm to 20 nm significantly stimulated signaling (6).

Intriguingly, the Hellmeier et al. study found that that origami platforms with a single native ligand (pMHC) could signal as efficiently as platforms containing neighboring ligand, unlike the results found with antibody ligands (6). Aside from the possibility that triggering by monovalent DNA origami may reflect an artifact due to transfer of peptides from the pMHC complex to MHC on

the surface of T cells for representation (41), this result indicates that pMHC interacts in some fundamentally different manner with TCR than nonnative ligands (DNA ligands or antibodies). The authors suggest that one pMHC might serially trigger and activate several TCRs in a catalytic manner and that these activated TCRs could organize into signal-promoting clusters. This is consistent with recent single-molecule imaging analyses, in which at low antigen density, TCRs were found not to be clustered during T cell activation (4) and interrogation of pMHC:TCR complexes reveals sparsely distributed monomeric interactions can lead to activation (5). Earlier studies by Manz et al. suggest that a minimum of four pMHC are needed in a 0.5 × 0.5 mm zone to trigger calcium signaling (12), but the Hellmeier study raises the possibility that even more TCRs might be activated in such a zone. The mechanism by which pMHC might trigger a prolonged activated state of the TCR even after ligand dissociation, the lifetime of that state, and whether/how nonligated and ligated activated TCRs might cluster remain open questions and constitute important topics for further investigation.

Nanoscale Patterning Controls the Time Course of Signaling Dynamics. A live cell readout of ERK signaling also allowed us to examine the effects of ligand patterns on signaling dynamics. First, we find that the ERK signaling is largely an all-or-none response and that the amplitude of the ERK signal is not affected by ligand density or spacing. These observations are consistent with a previous study showing that the ERK signaling cascade acts in a switch-like manner and converts the diverse ligand inputs into a full-magnitude intracellular signal (20). However, we find that different ligand patterns lead to distinct probabilistic and temporal dynamics of the ERK signals (Figs. 3 and 4).

We find that the number of ligands per origami affects the duration of the ERK response (Fig. 3). The duration of the ERK signaling has been proposed to be a key determinant of cell fate (33), such as cell proliferation (30), differentiation (32), and wound healing (31) in various cell types. In mature CD8+ T cells, durations of ERK correlate with specific T cell responses, in which strong and transient ERK activation induces apoptosis, whereas moderate but sustained ERK activation induces cell proliferation (42). ERK signal duration has also been shown to be required for thymocyte-positive selection in vivo (43). In addition to ligand concentration or type (32, 44), our results suggest spatial arrangement of ligands may be another parameter that can affect the ERK signaling response. Interestingly, at a fixed overall ligand number per cell, we find that small ligand clusters (4∼16 ligands) led to a longer-lasting ERK signal than larger ligand clusters (72 ligands) (Fig. 3 *C* and *D*). The mechanism of this effect is not known. One possibility is a feedback mechanism involving the tyrosine phosphatase SHP-1, which becomes rapidly activated upon receptor–ligand engagement and deactivates the TCR complex by dephosphorylation (19, 20). Large clusters may trap SHP-1, allowing it to serially dephosphorylate neighboring DNA-CARζ receptor more efficiently compared to the same number of receptors separated on separate origamis. However, other negative machineries, including the feedback loop from ERK to Raf (45), inhibitory factors proximal to the TCR signalosome (e.g., Csk) (46), and protein abundance regulation via ubiquitination (47) or ESCRT complex (48), may be involved in the effect that we observe on ERK signal timing.

We also show that ligand distancing delayed the initiation of the ERK response (Fig. 4 *B D*). This effect might be most relevant for T cell signaling in the context of their native tissue environments. Endogenous T cells move rapidly through the tissue (5 to 7 μm/min) (49) and have brief (<10 min) encounters with the antigen-presenting cells in secondary lymphoid organs (46). The delay in the response time of ERK signaling may provide stringent control for signaling noise (1). pMHCs of sufficient strength that stabilize TCRs into longer-lasting microclusters might trigger a rapid ERK response within the time window of engagement between a T cell and an antigen presenting cell (APC) in vivo.

Triggering Sensitivity to Strong Ligands Is Enhanced by Adjacent Weak Ligands. T cells deprived of self-recognition showed a loss in T cell signaling sensitivity in vivo (47), suggesting that the highly abundant endogenous pMHCs, though not stimulatory, may play an active role in signaling regulation. However, evidence for a signaling role of low-affinity pMHC is conflicting. Some studies suggest that low-affinity pMHC promote signaling by agonist pMHC (11, 20, 36), whereas other experiments observed no substantial impact (20, 37). One variable in these studies is the use of previously activated versus resting or naïve T cells; failure to see low-affinity ligand contribution was observed with naïve cells or previously activated cells rested for prolonged periods after initial stimulation, whereas cells tested in a narrow time period after initial activation did show responses to weak ligands (20). Jurkat, a continuously proliferating T cell tumor line, may have features closer to those of the activated cycling T cells than the resting T cells, hence the ability to sense weak ligands. These differences in T cell state aside, in these prior experiments, pMHCs of different affinities were typically assembled through chemical cross-linking, a method that lacks control over the stoichiometry or spatial organization, or simply offered to antigen-presenting cells.

We revisited the impact on signaling of low-affinity ligands using the DNA origami–based signaling system, which also offers the advantage of exploring the affinity and spatial arrangement of ligands. We demonstrate that, although weak ligands do not signal themselves, they can change the sensitivity, but not the timing, of ERK signaling by the strong ligands present at low density. This suggests that nontriggering weak ligands, which can nonetheless accumulate at the antigen-presenting cell interface (36), could contribute to the active signaling of T cells and enhance responses to strong ligands, especially at low densities. Additional insight into this phenomenon may have important implications for T cell immunotherapy, and future studies could explore this affect with weak and strong pMHCs bound to a DNA origami scaffold.

Other Uses of DNA Origami and Relevance for Immunotherapies. Our study, and other recent work (6), demonstrates the utility of DNA origami for probing the effects of nanoscale organization of membrane receptors on signaling, even in regimes that are lower than superresolution light microscopy. As we showed here, different types of ligands (here shown for high- and low-affinity ligands) can be patterned on a DNA origami surface. This approach could be extended to examine the effects of combining TCR and coreceptor ligands. In addition, it is possible to control the rigidity (50) and curvature of DNA origami structures (51). Such studies could probe the effects of substrate stiffness and native membrane topology, respectively, which have been suggested to have a significant impact on T cell recognition and activation (52).

Our findings and future studies with DNA origami may also have important ramifications for engineering biomolecules for therapeutic uses. For example, particles functionalized with agonistic antibodies have been used to drive ex vivo T cell expansion for adoptive cell therapy, a treatment that uses patient lymphocytes to eliminate cancer. In this method, the prevailing strategy to achieve signaling potency is to maximize the loading of agonistic antibodies on these particles. However, our results suggest that reducing ligand loading per particle could optimally tune the duration of activation of T cells to promote sustained cell survival and proliferation and avoid a strong but transient activation of ERK associated with apoptosis (42). Moreover, the spacing of agonistic antibodies on these particles also can be optimized to increase the probability of eliciting cellular signaling. We expect the methodology developed here would provide the basis for rapidly prototyping and optimizing nanoparticle reagents for immunotherapy.

Materials and Methods

DNA Origami Design and Preparation. The DNA origami pegboard was designed using version 2.2 of the Cadnano software (21). Optimization of staple routes was performed using a custom software toolkit developed in the S.M.D. laboratory. ssDNA scaffolds (Tilibit) and DNA staples (IDTDNA) were mixed at 5:1 molar ratio in $MgCl_2$-containing folding buffer and subjected to thermal denaturation-reannealing cycles. Folded DNA origamis were purified by polyethylene glycol (PEG) precipitation. To functionalize the glass surface with DNA origami, 96-well imaging plates (Brooks) were cleaned with Hellmanex (Sigma-Aldrich) and coated with Biotin-BSA followed by streptavidin (see *SI Appendix, Supplementary Materials and Methods* for details).

Cell Line Generation and Labeling. Jurkat cells were transduced with lentiviral vectors expressing DNA-CARζ, ERK-KTR-mScarlet, or the designated plasmid. Fluorescent cells were sorted 72 h after viral infection by flow cytometry.

ssDNA oligonucleotides of the DNA receptor strand were conjugated with benzylguanine (BG) via amine-ester reaction. To label DNA-CARζ–expressing cells with BG-labeled DNA receptor strands, cells were serum-deprived for 3 h, pelleted, and incubated with BG-labeled receptor DNA (10 μM) at room temperature for 15 min. Excess BG-labeled receptor DNAs were washed before using these cells for DNA origami stimulation experiments.

Microscopy. Imaging was performed on an inverted microscopy equipped with a spinning disk confocal and a TIRF combined system and μManager software for automatic multidimensional image acquisition.

Data Availability. All study data are included in the article and/or supporting information.

ACKNOWLEDGMENTS. We thank Xiaolei Su, Meghan Morrisey, Nadja Kern, and Chaim Gingold for constructive suggestions on this manuscript. R.D. was supported by a Jane Coffin Childs postdoctoral fellowship. T.A. was supported by a Ruth L. Kirschstein NRSA postdoctoral fellowship (F32GM119322) and the NSF (OAC-1740212). W.C. and R.N.G. were supported by the Intramural Research Program of the National Institute of Allergy and Infectious Diseases, NIH. R.D.V. is an investigator of the Howard Hughes Medical Institute. S.M.D. was supported by the Army Research Office (W911NF-14-1-0507) and Office of Naval Research (N00014-17-1-2627).

1. H. Wu, Higher-order assemblies in a new paradigm of signal transduction. *Cell* **153**, 287–292 (2013).
2. B. F. Lillemeier *et al*., TCR and Lat are expressed on separate protein islands on T cell membranes and concatenate during activation. *Nat. Immunol.* **11**, 90–96 (2010).
3. E. Sherman *et al*., Functional nanoscale organization of signaling molecules downstream of the T cell antigen receptor. *Immunity* **35**, 705–720 (2011).
4. J. J. Y. Lin *et al*., Mapping the stochastic sequence of individual ligand-receptor binding events to cellular activation: T cells act on the rare events. *Sci. Signal.* **12**, eaat8715 (2019).
5. M. Brameshuber *et al*., Monomeric TCRs drive T cell antigen recognition. *Nat. Immunol.* **19**, 487–496 (2018).
6. J. Hellmeier *et al*., DNA origami demonstrate the unique stimulatory power of single pMHCs as T cell antigens. *Proc. Natl. Acad. Sci. U.S.A.* **118**, e2016857118 (2021).
7. A. D. Douglass, R. D. Vale, Single-molecule microscopy reveals plasma membrane microdomains created by protein-protein networks that exclude or trap signaling molecules in T cells. *Cell* **121**, 937–950 (2005).
8. E. Hui, R. D. Vale, In vitro membrane reconstitution of the T-cell receptor proximal signaling network. *Nat. Struct. Mol. Biol.* **21**, 133–142 (2014).
9. M. J. Taylor, K. Husain, Z. J. Gartner, S. Mayor, R. D. Vale, A DNA-based T cell receptor reveals a role for receptor clustering in ligand discrimination. *Cell* **169**, 108–119.e20 (2017).
10. J. R. Cochran, T. O. Cameron, J. D. Stone, J. B. Lubetsky, L. J. Stern, Receptor proximity, not intermolecular orientation, is critical for triggering T-cell activation. *J. Biol. Chem.* **276**, 28068–28074 (2001).
11. M. Krogsgaard *et al*., Agonist/endogenous peptide-MHC heterodimers drive T cell activation and sensitivity. *Nature* **434**, 238–243 (2005).
12. B. N. Manz, B. L. Jackson, R. S. Petit, M. L. Dustin, J. Groves, T-cell triggering thresholds are modulated by the number of antigen within individual T-cell receptor clusters. *Proc. Natl. Acad. Sci. U.S.A.* **108**, 9089–9094 (2011).
13. H. Cai *et al*., Full control of ligand positioning reveals spatial thresholds for T cell receptor triggering. *Nat. Nanotechnol.* **13**, 610–617 (2018).
14. J. Deeg *et al*., T cell activation is determined by the number of presented antigens. *Nano Lett.* **13**, 5619–5626 (2013).
15. D. Delcassian *et al*., Nanoscale ligand spacing influences receptor triggering in T cells and NK cells. *Nano Lett.* **13**, 5608–5614 (2013).
16. A. J. Ben-Sasson *et al*., Design of biologically active binary protein 2D materials. *Nature* **589**, 468–473 (2021).
17. P. W. Rothemund, Folding DNA to create nanoscale shapes and patterns. *Nature* **440**, 297–302 (2006).
18. A. Shaw *et al*., Binding to nanopatterned antigens is dominated by the spatial tolerance of antibodies. *Nat. Nanotechnol.* **14**, 184–190 (2019).
19. I. Stefanová *et al*., TCR ligand discrimination is enforced by competing ERK positive and SHP-1 negative feedback pathways. *Nat. Immunol.* **4**, 248–254 (2003).
20. G. Altan-Bonnet, R. N. Germain, Modeling T cell antigen discrimination based on feedback control of digital ERK responses. *PLoS Biol.* **3**, e356 (2005).
21. S. M. Douglas *et al*., Rapid prototyping of 3D DNA-origami shapes with caDNAno. *Nucleic Acids Res.* **37**, 5001–5006 (2009).
22. J. Jayaraman *et al*., CAR-T design: Elements and their synergistic function. *EBioMedicine* **58**, 102931 (2020).
23. L. Yao *et al*., Application of SNAP-tag in expansion super-resolution microscopy using DNA oligostrands. *Front Chem.* **9**, 640519 (2021).
24. A. Kuzuya, K. Numajiri, M. Kimura, M. Komiyama, Single-molecule accommodation of streptavidin in nanometer-scale wells formed in DNA nanostructures. *Nucleic Acids Symp Ser (Oxf)* **52**, 681–682 (2008).
25. P. G. Squire, P. Moser, C. T. O'Konski, The hydrodynamic properties of bovine serum albumin monomer and dimer. *Biochemistry* **7**, 4261–4272 (1968).
26. B. N. Dittel, I. Stefanova, R. N. Germain, C. A. Janeway Jr, Cross-antagonism of a T cell clone expressing two distinct T cell receptors. *Immunity* **11**, 289–298 (1999).
27. D. R. Plas *et al*., Direct regulation of ZAP-70 by SHP-1 in T cell antigen receptor signaling. *Science* **272**, 1173–1176 (1996).
28. S. Murugesan *et al*., Formin-generated actomyosin arcs propel T cell receptor microcluster movement at the immune synapse. *J. Cell Biol.* **215**, 383–399 (2016).
29. S. Regot, J. J. Hughey, B. T. Bajar, S. Carrasco, M. W. Covert, High-sensitivity measurements of multiple kinase activities in live single cells. *Cell* **157**, 1724–1734 (2014).
30. A. G. Goglia *et al*., A live-cell screen for altered Erk dynamics reveals principles of proliferative control. *Cell Syst.* **10**, 240–253.e6 (2020).
31. T. Hiratsuka *et al*., Intercellular propagation of extracellular signal-regulated kinase activation revealed by in vivo imaging of mouse skin. *eLife* **4**, e05178 (2015).
32. C. de la Cova, R. Townley, S. Regot, I. Greenwald, A real-time biosensor for ERK activity reveals signaling dynamics during *C. elegans* cell fate specification. *Dev. Cell* **42**, 542–553.e4 (2017).
33. L. O. Murphy, J. Blenis, MAPK signal specificity: The right place at the right time. *Trends Biochem. Sci.* **31**, 268–275 (2006).
34. R. J. Martinez, B. D. Evavold, Lower affinity T cells are critical components and active participants of the immune response. *Front. Immunol.* **6**, 468 (2015).
35. M. A. Purbhoo *et al*., Quantifying and imaging NY-ESO-1/LAGE-1-derived epitopes on tumor cells using high affinity T cell receptors. *J. Immunol.* **176**, 7308–7316 (2006).
36. C. Wülfing *et al*., Costimulation and endogenous MHC ligands contribute to T cell recognition. *Nat. Immunol.* **3**, 42–47 (2002).
37. R. Spörri, C. Reis e Sousa, Self peptide/MHC class I complexes have a negligible effect on the response of some CD8+ T cells to foreign antigen. *Eur. J. Immunol.* **32**, 3161–3170 (2002).
38. G. P. O'Donoghue, R. M. Pielak, A. A. Smoligovets, J. J. Lin, J. T. Groves, Direct single molecule measurement of TCR triggering by agonist pMHC in living primary T cells. *eLife* **2**, e00778 (2013).
39. D. Dong *et al*., Structural basis of assembly of the human T cell receptor-CD3 complex. *Nature* **573**, 546–552 (2019).
40. S. V. Pageon *et al*., Functional role of T-cell receptor nanoclusters in signal initiation and antigen discrimination. *Proc. Natl. Acad. Sci. U.S.A.* **113**, E5454–E5463 (2016).
41. Q. Ge *et al*., Soluble peptide-MHC monomers cause activation of CD8+ T cells through transfer of the peptide to T cell MHC molecules. *Proc. Natl. Acad. Sci. U.S.A.* **99**, 13729–13734 (2002).
42. X. Wang *et al*., Dynamics of proximal signaling events after TCR/CD8-mediated induction of proliferation or apoptosis in mature CD8+ T cells. *J. Immunol.* **180**, 6703–6712 (2008).
43. L. K. McNeil, T. K. Starr, K. A. Hogquist, A requirement for sustained ERK signaling during thymocyte positive selection in vivo. *Proc. Natl. Acad. Sci. U.S.A.* **102**, 13574–13579 (2005).
44. B. Lim *et al*., Dynamics of inductive ERK signaling in the *Drosophila* embryo. *Curr. Biol.* **25**, 1784–1790 (2015).
45. H. Ryu *et al*., Frequency modulation of ERK activation dynamics rewires cell fate. *Mol. Syst. Biol.* **12**, 866 (2016).
46. S. Simoncelli *et al*., Multi-color molecular visualization of signaling proteins reveals how C-terminal Src kinase nanoclusters regulate T cell receptor activation. *Cell Rep.* **33**, 108523 (2020).
47. M. Naramura *et al*., c-Cbl and Cbl-b regulate T cell responsiveness by promoting ligand-induced TCR down-modulation. *Nat. Immunol.* **3**, 1192–1199 (2002).
48. S. Vardhana, K. Choudhuri, R. Varma, M. L. Dustin, Essential role of ubiquitin and TSG101 protein in formation and function of the central supramolecular activation cluster. *Immunity* **32**, 531–540 (2010).
49. R. N. Germain, E. A. Robey, M. D. Cahalan, A decade of imaging cellular motility and interaction dynamics in the immune system. *Science* **336**, 1676–1681 (2012).
50. R. M. Zadegan *et al*., Twisting of DNA origami from intercalators. *Sci. Rep.* **7**, 7382 (2017).
51. T. Gerling, M. Kube, B. Kick, H. Dietz, Sequence-programmable covalent bonding of designed DNA assemblies. *Sci. Adv.* **4**, eaau1157 (2018).
52. J. Pettmann, A. M. Santos, O. Dushek, S. J. Davis, Membrane ultrastructure and T cell activation. *Front. Immunol.* **9**, 2152 (2018).